ACCOUNTS
of chemical research

Theranostic Magnetic Nanoparticles

DONGWON YOO, JAE-HYUN LEE, TAE-HYUN SHIN, AND JINWOO CHEON*

Department of Chemistry, Yonsei University, Seoul 120-749, Korea

RECEIVED ON MARCH 16, 2011

CONSPECTUS

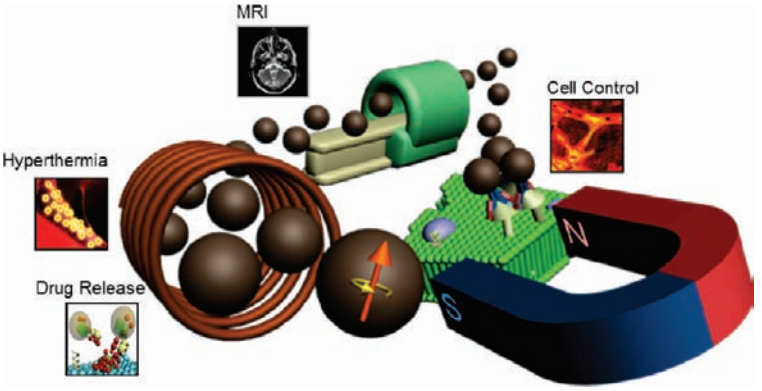

Early detection and treatment of disease is the most important component of a favorable prognosis. Biomedical researchers have thus invested tremendous effort in improving imaging techniques and treatment methods. Over the past decade, concepts and tools derived from nanotechnology have been applied to overcome the problems of conventional techniques for advanced diagnosis and therapy. In particular, advances in nanoparticle technology have created new paradigms for theranostics, which is defined as the combination of therapeutic and diagnostic agents within a single platform. In this Account, we examine the potential advantages and opportunities afforded by magnetic nanoparticles as platform materials for theranostics.

We begin with a brief overview of relevant magnetic parameters, such as saturation magnetization, coercivity, and magnetocrystalline anisotropy. Understanding the interplay of these parameters is critical for optimizing magnetic characteristics needed for effective imaging and therapeutics, which include magnetic resonance imaging (MRI) relaxivity, heat emission, and attractive forces. We then discuss approaches to constructing an MRI nanoparticle contrast agent with high sensitivity. We further introduce a new design concept for a fault-free contrast agent, which is a *T*1 and *T*2 dual mode hybrid.

Important capabilities of magnetic nanoparticles are the external controllability of magnetic heat generation and magnetic attractive forces for the transportation and movement of biological objects. We show that these functions can be utilized not only for therapeutic hyperthermia of cancer but also for controlled release of cancer drugs through the application of an external magnetic field. Additionally, the use of magnetic nanoparticles to drive mechanical forces is demonstrated to be useful for molecular-level cell signaling and for controlling the ultimate fate of the cell. Finally, we show that targeted imaging and therapy are made possible by attaching a variety of imaging and therapeutic components. These added components include therapeutic genes (small interfering RNA, or siRNA), cancer-specific ligands, and optical reporting dyes. The wide range of accessible features of magnetic nanoparticles underscores their potential as the most promising platform material available for theranostics.

1. Introduction

Although cancer is one of the leading causes of death, treatment options are limited and accurate diagnosis and prognosis are difficult in many cases. Therefore, tremendous efforts in biomedical research have been devoted to improving the sensitivity and accuracy of the diagnosis with the aim of early diagnosis and possibly better efficacy of the treatment methods. Recently, nanotechnology has served a new role in biomedical sciences by providing a variety of nanotechnology platforms.[1] Nanoplatform materials are generally categorized as either organic or inorganic materials. Typical organic platforms include polymer–drug conjugates, polymeric micelles, and dendrimers and are used primarily for drug delivery. For example, Abraxane, nanoparticle albumin bound (nab)

Published on the Web 08/08/2011 www.pubs.acs.org/accounts
10.1021/ar200085c

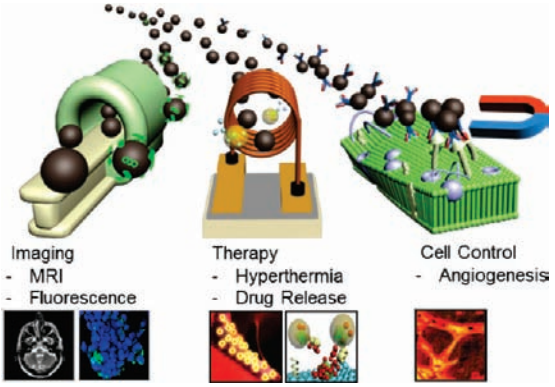

FIGURE 1. Magnetic nanoparticles are versatile platform materials suitable for theranostics. Targeted imaging, thermal therapy, precise drug release, and cell signaling controls are all possible.

paclitaxel, is the first drug in this class approved by the United States Food and Drug Administration (FDA) for breast cancer.[2a] With the advantages of increased drug efficacy and less toxicity, now various organic nanoplatform drugs are being tested in clinical trials.[2b] Compared to organic nanoparticles, inorganic nanoparticles have more diverse and distinct physical properties contingent to their size and composition.[3] In particular, magnetic nanoparticles exhibit not only unique material properties but also an integrated design capability for cell targeting, imaging, and therapy, which render them as ideal platform materials for theranostics.[4] While iron oxide based magnetic nanoparticles were first utilized as *T*2-MRI contrast agent, a number of new magnetic variants have been introduced to improve the signal sensitivity for better MRI diagnostics. In addition, these nanoparticle platforms can accommodate other complementary imaging modalities, therapeutic drugs, and targeting ligands and then can achieve highly accurate imaging and effective therapeutic goals. Moreover, the magnetic nanoparticle platforms can act as magnetic switches for molecular level control of cell signaling and functions. In this Account, we first provide a brief background on the physical parameters of magnetic nanoparticles and then introduce design strategies for magnetic nanoparticles as a platform for contrast agents to achieve highly accurate and early MRI diagnosis. Not only will we discuss the incorporation of conventional drugs and genes with magnetic nanoplatforms for selective cell targeting and drug delivery, but also further integration of new functions will be discussed for mechanical actuation and manipulation of drug release and control of cellular activities, which are important to accomplish high efficacy therapeutics in a noninvasive and remote fashion. The overall scheme of the theranostic magnetic nanoparticles is given in Figure 1.

2. Magnetism for Biomedical Studies

The characteristics of magnetic nanoparitcles are usually measured by magnetization (M), coercivity (H_c), and magnetocrystalline anisotropy constant (K).[5] Saturation magnetization (M_s) is the maximum magnetization value of a nanoparticle under a high magnetic field. Coercivity (H_c) is the strength of the external magnetic field to make the magnetization value of subjective nanoparticles zero. The zero coercivity of a superparamagnetic nanoparticle is essential for biomedical studies where no residual magnetization is critical in preventing their coagulation and sustaining a long period of circulation in the body. Magnetocrystalline anisotropy is the tendency of the magnetization to align itself along a preferred crystallographic direction of easy axis. The magnetocrystalline anisotropy constant (K) is a physical constant which reflects the energy required to change the direction of magnetization from easy to hard axis.

Table 1 summarizes the relationship of magnetic parameters to magnetic resonance imaging (MRI) sensitivity, heat generation, and magnetic attraction force. Under external magnetic field, magnetic nanoparticles generate a secondary magnetic field, which can cause a faster relaxation time ($T2$) of the protons in the water molecules. The transverse relaxation rate ($R2$), which is defined as $1/T2$ and the sensitivity indicator of the MRI contrast agent for $T2$ imaging, is shown in eq 1. Graphs (a) and (b) predict that a high M_s and large particle size (r) are necessary for a higher $R2$. Not just only for imaging contrast enhancements, magnetic nanoparticles can perform as an energy transfer mediator and as a mechanical force vector. Through repeated alignments of magnetic spins and relaxations via Néel (spin rotation) and Brownian (particle rotation) processes in response to the alternating magnetic field, thermal energy can be dissipated from the magnetic nanoparticles. The gauge of such a property is known as the specific loss power (SLP) which is measured as the initial temperature rise of the nanoparticle solution per unit volume or mass. SLP is dependent on the volume, M_s, and K (eqs 2 and 3 in Table 1). While the SLP value can have a maximum point at a certain particle size (r) and K (graph (d) in Table 1),[6] it is proportional to M_s (graph (e) in Table 1).[6,7] The typical SLP value of iron-oxide-based magnetic nanoparticles ranges from 100 to 500 W/g, which is still low and needs to be improved upon for successful clinical trials.[8]

The magnetic manipulation of nanoparticles as translational vectors can be uniquely important in their biological

TABLE 1. Functional Properties of Magnetic Nanoparticles

	Equation[a]	Relationship with Nanoparticle Properties
MRI Relaxivity (*R2*)[10]	$R2 = \frac{1}{T2} = \frac{256\pi^2\gamma^2}{405} M_s^2 V^* \frac{r^2}{D(1+L/r)}$ (1)	(a) *R2* vs size (*r*); (b) *R2* vs magnetization (M_s)
Heat Emission (SLP)[7]	$\mathrm{SLP} = \frac{\mu_0 H M_s}{2\rho} L(\xi) \frac{\omega^2\tau}{1+(\omega\tau)^2}$ (2); $\frac{1}{\tau} = \frac{1}{\tau_0 e^{KV/kT}} + \frac{kT}{3\eta V}$ (3)	(c) SLP vs size (*r*); (d) SLP vs magnetic anisotropy (*K*); (e) SLP vs magnetization (M_s)
Translational Attractive Force (F_m)[11]	$F_m = V(M_s \cdot \nabla)B$ (4)	(f) F_m vs size (*r*); (g) F_m vs magnetization (M_s)

[a] *T*2, transverse relaxation time; γ, proton gyromagnetic ratio; M_s, saturation magnetization; V^*, nanoparticle volume fraction; *r*, nanoparticle core radius; *D*, diffusivity of water molecule; *L*, thickness of surface coating; SLP, specific loss power; μ_0, vacuum permeability; *H*, magnetic field strength; ρ, density of particle; $L(\xi)$, Langevin function; ω, angular frequency; τ, relaxation time; *K*, magnetic anisotropy constant; *k*, Boltzmann constant; *V*, particle volume; η, viscosity of solution; F_m, force experienced by a particle; *B*, magnetic field intensity.

applications such as drug delivery[9a] and mechanical cell signaling.[9b] The attractive force that can be exerted to the magnetic nanoparticles by an external field is given by eq 4 in Table 1 where high magnetization and larger size are necessary to ensure a strong attractive force (graphs (f), (g)). However, the size of the magnetic nanoparticles should remain small enough to be within the regime of the superparamagnetism.

3. Magnetic Nanoparticles for Imaging Diagnostics

Early and accurate diagnosis of diseases or biological targets is very important because the treatments are simpler and more effective when diagnosed at an early stage. Unfortunately, many types of cancers such as pancreatic cancer are still very difficult to detect until their later stages. Due to high imaging contrast effects, magnetic nanoparticles can increase the difference between pathogenic targets and normal tissues via MRI. The relaxivity coefficient (*r*2) of contrast agents can be tuned and further enhanced by engineering magnetic parameters. We first describe an approach known as magnetic spin modulation to increase *r*2. Since MRI sensitivity alone is not perfect for early diagnosis, a new methodology for achieving higher accuracy in the diagnosis is equally important. Most MRI inaccuracy comes from various artifacts present in physiological conditions, such as incomplete fat suppression, air bubbles in the bloodstream, and calcification. These undesired artifacts are present in the MR images of the targeted areas on many occasions,[12] and therefore, the development of the next generational MR imaging agents is important. We introduce a new design concept which is an "AND" logic *T*1/*T*2 dual mode contrast agent which can significantly increase the degree of accuracy in imaging diagnosis.

3.1. Magnetic Nanoparticles with High MRI Sensitivity. To detect small sized pathogenic targets precisely at an early stage, MRI contrast agents are often used to highlight those specific areas of interest. One of the most effective ways to increase the MR contrast effects is the optimization of saturation magnetization (M_s) which is directly related to the relaxivity coefficient (*r*2). The relaxivity coefficient (*r*2) is determined by a slope of *R2* against nanoparticle concentration and occasionally used as an indicator for contrast effects. The magnetism engineering of iron oxide nanoparticles has already been reported where substitution of one of the Fe ions with different magnetic atoms such as Mn can increase the M_s. Here we describe even more pronounced contrast effects are possible when nonmagnetic atoms replace the Fe ions.[13] The scheme for magnetic tunability of Zn^{2+} doped ferrite nanoparticles is depicted in Figure 2.

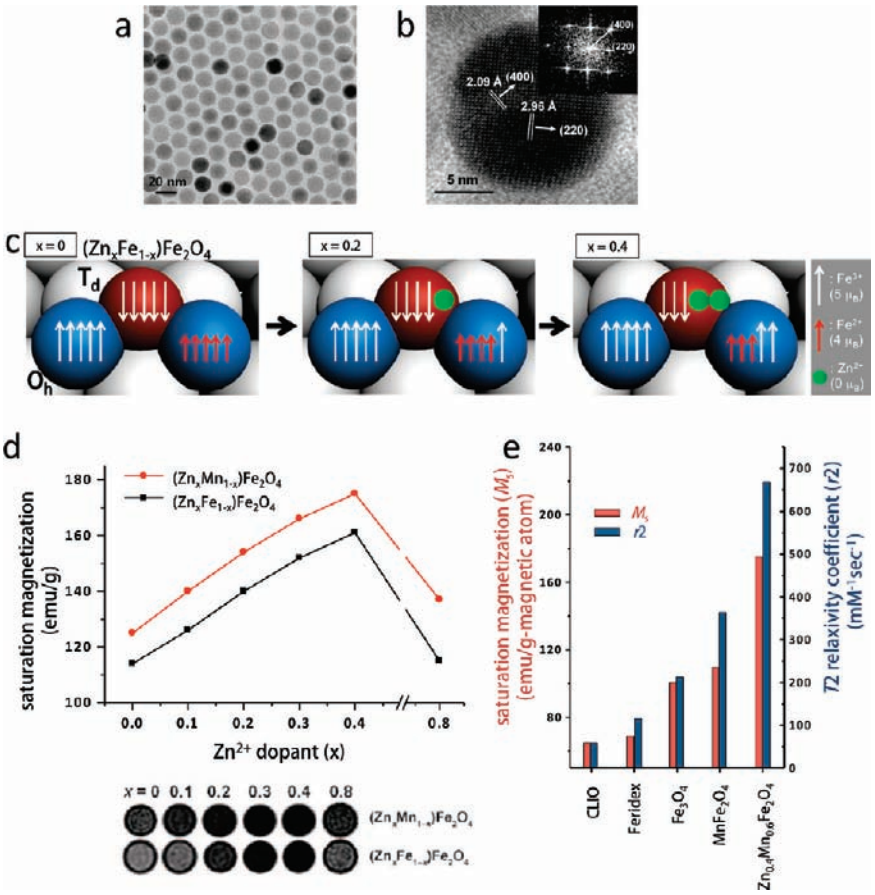

FIGURE 2. Zn-doped magnetic nanoparticles for strong MRI contrast effect. Low (a) and high (b) resolution TEM images of 15 nm $(Zn_{0.4}Fe_{0.6})Fe_2O_4$ nanoparticles. The inset shows the fast Fourier transform (FFT) pattern revealing its inverse spinel structure. (c) Undoped ($x = 0$) and Zn^{2+} doped ($x =$ 0.2, 0.4) magnetic spin alignment diagrams of inverse spinel-structured nanoparticles under magnetic field. (d) Graphs of M_s versus $(Zn_xM_{1-x})Fe_2O_4$ ($M = Mn^{2+}$ (red line), Fe^{2+} (black line)) nanoparticles. *T*2-weighted MR images of $(Zn_xM_{1-x})Fe_2O_4$ are shown on the bottom. (e) Graphs of M_s and *r*2 values of representative nanoparticles.

Transmission electron microscopy (TEM) images of 15 nm $(Zn_{0.4}Fe_{0.6})Fe_2O_4$ nanoparticles show the monodispersity and single crystalline spinel structure (Figure 2a,b). By substituting Fe^{2+} in the T_d holes with nonmagnetic Zn^{2+} (0 μ_B), the antiparallel spin interactions between the magnetic ions in the O_h holes and T_d holes are reduced, which results in an increase of the net magnetic magnetization of the nanoparticles (Figure 2c). As shown in Figure 2d, M_s increases with Zn^{2+} doping and becomes maximum with a Zn^{2+} of 0.4 in $(Zn_xM_{1-x})Fe_2O_4$ ($M = Mn^{2+}$, Fe^{2+}) and then decreases. The modulation of M_s values directly generates enhanced contrast effects where the relaxivity coefficient (*r*2) increases significantly from less than 100 to almost 700 mM^{-1} s^{-1} as seen Figure 2e. For example, for $(Zn_{0.4}Mn_{0.6})Fe_2O_4$ nanoparticles with a high M_s value of 175 emu/g-magnetic atom, the *r*2 reaches up to 676 mM^{-1} s^{-1} which is 6 times higher than that of Feridex which is one of the most representative iron-oxide based contrast agents.[13]

3.2. Design of Accurate MRI Contrast Agent: Is Fault-Free MRI Possible? Conventional MRI contrast agents are mostly effective only in a single imaging mode of either *T*1 or *T*2 and frequently suffer the ambiguities in diagnostics especially for small biological targets. The combination of simultaneously strong *T*1 and *T*2 contrast effects in a single contrast agent can be one of the new breakthroughs, since it can potentially provide more accurate MR imaging via self-confirmation with better differentiation of normal and diseased areas (Figure 3a). However, the realization of such contrast has been challenging.[14] Due to the strong magnetic coupling between the contrast agents of *T*1 and *T*2 when they are in proximity, the spin−lattice relaxation processes of *T*1 contrast materials is significantly diminished (Figure 3b). One of the strategies to overcome such a phenomenon is the inclusion of a separation layer to modulate their magnetic couplings. For example, micellar structures using organic block copolymers, inorganic porous

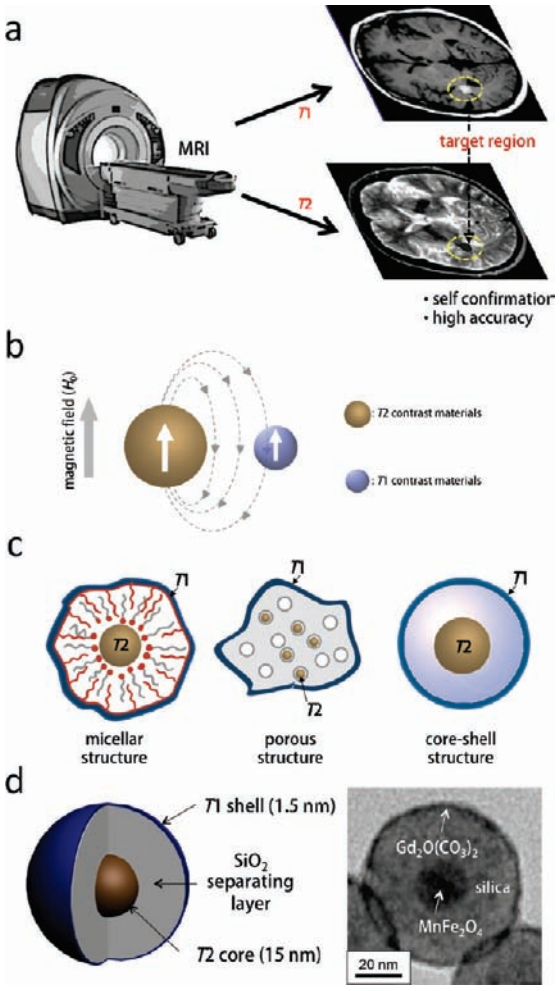

FIGURE 3. Dual mode scheme for MRI for highly accurate imaging. (a) DMCA is responsive with ON signals for a bright image in the *T*1 mode and a dark image in the *T*2 mode, which renders self-confirmation capability via overlay of the images. The MR images are added with artificial drawings to demonstrate the concept of the dual mode contrast agent. (b) Electronic spins of *T*1 contrast materials are affected by a magnetic field from *T*2 contrast materials when they are in close proximity. (c) Possible structures for a *T*1/*T*2 dual mode nanoparticle contrast agent with separating layers. (d) Schematic and TEM image of core–shell type DMCA [$MnFe_2O_4$@SiO_2@$Gd_2O(CO_3)_2$].

materials such as MCM-48, and core–shell type inorganic materials are possible frameworks for such a purpose (Figure 3c). Among these, we introduce a core–shell type *T*1–*T*2 dual mode nanoparticle contrast (DMCA) agent,[15] where the *T*1 contrast material is positioned on the shell to have direct contact with water for high *T*1 contrast effects and the superparamagnetic *T*2 contrast material is located in the core, inducing a long-range magnetic field for the relaxation of water. Fifteen nm $MnFe_2O_4$ is used as the *T*2 material and 1.5 nm $Gd_2O(CO_3)_2$ is coated as the *T*1 material (Figure 3d). The two materials are separated by SiO_2. By adjusting the thickness of the SiO_2, the magnetic coupling between *T*1 and *T*2 contrast materials is controlled (Figure 4a,b). As the SiO_2 becomes thicker, *T*1 quenching reduces and, concurrently, *r*1 increases while the decrement of the *T*2 effects is relatively weaker (Figure 4b). When the SiO_2 layer is 16 nm, both T*1* and *T*2 contrast effects become larger than the effects of the well-known single mode contrast agents, Gd-DTPA and Feridex. Due to the simultaneously high *T*1 and *T*2 effect, DMCA can now be used effectively to perform "AND" logic in MRI. In the *T*1 mode, both DMCA and Gd-DTPA display bright "ON" signals while water and Feridex display dark "OFF" signals. In the *T*2 mode, DMCA and Feridex display dark "ON" signals while water and Gd-DTPA display bright "OFF" signals (Figure 4c). Only the DMCA possesses "AND" logic, which gives MRI a self-confirmation capability. Figure 4d shows MR images of a mouse where 1 mm diameter tubings containing DMCA, Feridex, and Gd-DTPA are implanted. Gd-DTPA and DMCA exhibit 30% and 35% *T*1-relaxivity change. In terms of *T*2-relaxivity change, Feridex and DMCA show 35% and 72% relaxivity change, respectively. Only DMCA displays high MR signals in both *T*1 and *T*2 modes. Therefore, we can compare changes between the pre- and postcontrast MR images and then exclude any faulty signals. Since potential ambiguity of the single mode contrast agent from artifacts present in vivo can be eliminated, this study indicates that the dual-mode contrast concept for MRI can bring about enhanced diagnostic accuracy.

4. Magnetic Nanoparticles as Smart Actuators and Carrier Vectors for Therapeutics

As opposed to most other imaging agents, magnetic nanoparticles are unique in that these can be used as a means for actuation such as heat generation and translational vectors for spatial movements. These can be done remotely and noninvasively. Here, we demonstrate four different cases. Not only can magnetic nanoparticles be functional by themselves such as magnetic hyperthermia for cancer treatment, but they can also be useful as a drug carrier and an actuator for controlled drug release. Magnetically driven mechanical forces can selectively be applied to control certain biological functions to determine their cell growth or death. We show that angiogenesis related cellular growth is possible using magnetic nanoparticles as a remote mechanical actuator. Lastly, these magnetic nanoparticles are highly effective carrier platforms for both reporting and therapeutic purposes by carrying various bioactive molecules such as genes and imaging probes.[16]

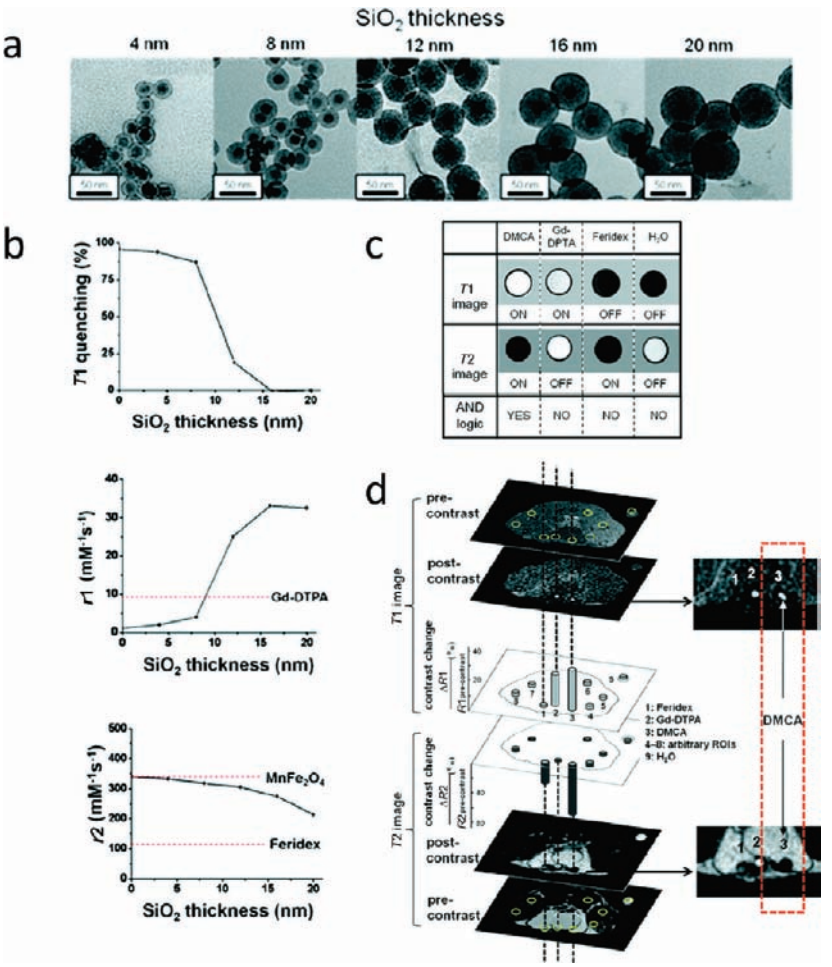

FIGURE 4. *T*1−*T*2 dual mode nanoparticle contrast agent (DMCA). (a) TEM images of DMCA with variable separating layer thickness (4, 8, 12, 16, and 20 nm), having a fixed $MnFe_2O_4$ core (15 nm in diameter) and a $Gd_2O(CO_3)_2$ shell (1.5 nm). (b) Graphs of *T*1 quenching, *r*1, *r*2 vs SiO_2 thickness. (d) *T*1- and *T*2-weighted MR images of DMCA [$MnFe_2O_4$@SiO_2@$Gd_2O(CO_3)_2$, $SiO_2 = 16$ nm], Feridex, Gd-DTPA (diethyltriaminepentaacetic acid), and water. (c) *T*1- and *T*2-weighted transverse MR images of a mouse where 1 mm diameter tubings containing DMCA, Feridex, and Gd-DTPA are implanted near the abdomen. Only DMCA exhibits a simultaneously high signal in both *T*1 and *T*2.

4.1. Hyperthermia with Enhanced Performance. Magnetically induced heat generation from nanoparticles can be used for various purposes including disease therapy known as hyperthermia. Such therapeutic capability is dependent on the specific loss power (SLP). The strategy for enhancing SLP has been important, since high SLP can bring better efficacy with a lower dosage level of nanoparticles. Upon exposure to the alternating external magnetic field, the magnetic nanoparticles continuously emit heat via Néel and Brownian pathways (Figure 5a). The hyperthermia device consists of the RLC (resistor, inductor, and capacitor) circuit causing the induction of an AC field with a frequency of 100 kHz to 1 MHz and an amplitude of 10−50 kA/m. The water-jacketed coil is usually used to cool down the coil temperature (Figure 5b). As described in section 2, the SLP values are proportional to the M_s values but inversely proportional to the size distribution of the nanoparticles (σ). SLP values have a maximum point at certain particle size and magnetocrystalline anisotropy constant (*K*). Therefore, magnetic nanoparticles with high M_s values, an optimal anisotropy constant (*K*), and high monodispersity are desirable for effective hyperthermia.

The nanoparticles that we described in the previous section are Zn ion doped iron oxide nanoparticles $(Zn_{0.4}Mn_{0.6})Fe_2O_4$ with a large M_s value of 175 emu/g-magnetic atom and high monodispersity ($\sigma < 5\%$), and they seem to be promising candidates for hyperthermia.[13] In fact, the measured SLP value of $(Zn_{0.4}Mn_{0.6})Fe_2O_4$ is 432 W/g which is ~4 times larger than that (115 W/g) of Feridex measured at 500 kHz and 37 kA/m (Figure 5c). The use of such magnetic nanoparticles with high SLP indeed has high efficacy for hyperthermia in cancer cell studies. Whereas only 13.5% of HeLa cancer cells die in the

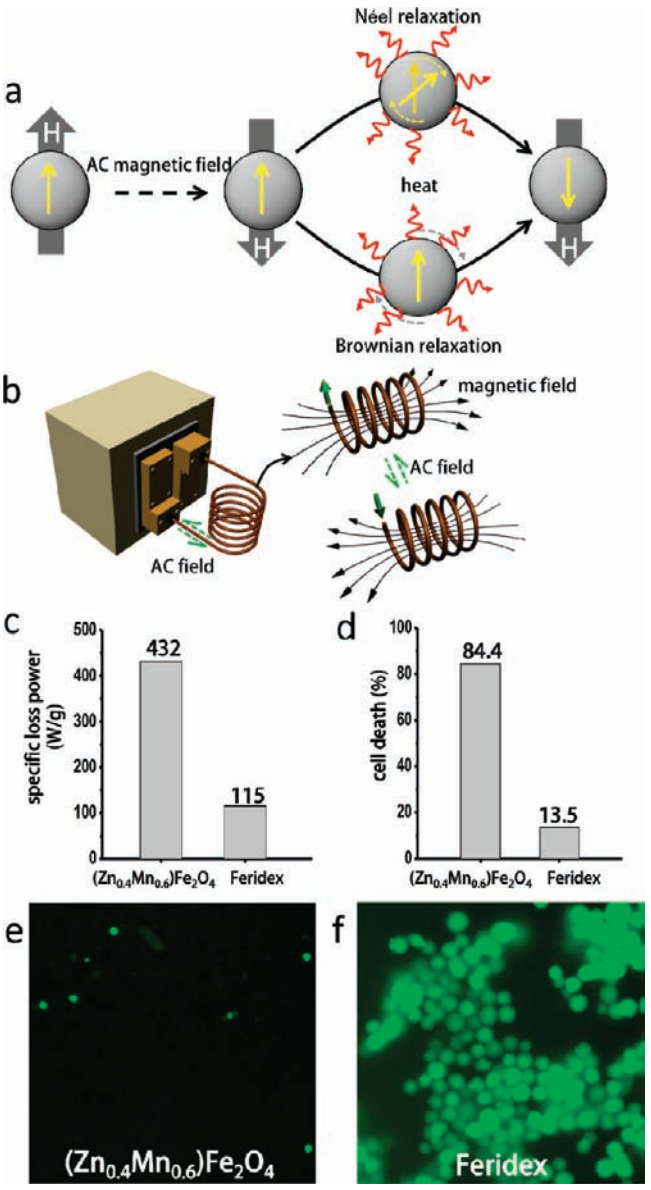

FIGURE 5. Magnetic nanoparticles for hyperthermia. (a) Néel and Brownian relaxation processes. (b) Experimental apparatus. (c) SLP values for $(Zn_{0.4}Mn_{0.6})Fe_2O_4$ and Feridex in a 500 kHz AC magnetic field with an amplitude of 37 kA/m. (d) Percentage of HeLa cells killed after hyperthermic treatment with $(Zn_{0.4}Mn_{0.6})Fe_2O_4$ nanoparticles and Feridex. Fluorescence microscopy images of HeLa cells treated with (e) $(Zn_{0.4}Mn_{0.6})Fe_2O_4$ nanoparticles and (f) Feridex.

case of Feridex, 84.4% of those cells treated with $(Zn_{0.4}Mn_{0.6})Fe_2O_4$ are dead 10 min after the application of the AC magnetic field (Figure 5d). Here, the viability of cells upon hyperthermia treatment with magnetic nanoparticles is examined by fluorescence microscope images, in which live cells are stained with calcein emitting green fluorescence (Figure 5e,f).

4.2. Magnetically Controlled Drug Release. Controlled drug release in a remote and noninvasive fashion is very important for theranostics.[17] The thermal energy from magnetic nanoparticles can be used as an external and remotely controlled trigger for controlled drug release. For example, the thermal energy can open the gates of any kind of organic or inorganic carriers which contain drugs for therapy. Specifically, 15 nm $(Zn_{0.4}Fe_{0.6})Fe_2O_4$ nanoparticles with a high SLP value described in the previous section are incorporated inside porous drug carrier nanoparticles with molecular valves.[18] A molecular valve, which consists of a thread and capping molecule (cucurbit[6]uril), closes the silica pores to keep the drug inside (Figure 6a,b). When an external alternating magnetic field is applied, heat generation and a subsequent pressure buildup (~90 bar) inside the porous nanoparticles cause the rapid removal of the molecular valves and the release of the cargo (Figure 6b). Figure 6cis a TEM image of $(Zn_{0.4}Fe_{0.6})Fe_2O_4$ nanoparticles encapsulated by mesoporous silica nanoparticles. The controlled cargo release is demonstrated by the application of a pulsed magnetic field where the release of a fluorescent dye (Rhodamine B) is observed in each pulse in a staircase-like fashion (Figure 6d). The first pulse releases ~40% of the cargo. Doxorubicin and magnetic nanoparticles loaded porous nanoparticles with FITC (fluorescein isothiocyanate) for green fluorescence are tested for the treatment of cancer cells (Figure 6e). The top image of Figure 6e is the control fluorescence image of breast cancer cells transfected only with silica nanoparticles. After the MDA-MB-231 breast cancer cells are transfected with the nanoparticles, yellow fluorescence regions indicate overlap of the red fluorescence from doxorubicin with the green fluorescence from the silica nanoparticles. When cells transfected with silica nanoparticles containing doxorubicin are treated with an AC field, red fluorescence from the released doxorubicin from the silica particles and cell shrinkage and death are apparently observed.[18] This result indicates that magnetic nanoparticles are effective as an actuator for controlled drug release from a carrier in a noninvasive and remote way.

4.3. Magnetic Switches for Cell Fate Control. Magnetic nanoparticles are also used to generate mechanical stimulations on cells, which can induce changes in cell activity such as differentiation, growth, and death.[19] Under an external magnetic field, magnetic nanoparticles can move around on cell membrane surfaces and exert translational forces. Simultaneously, magnetic nanoparticles with specific ligands can bind to certain receptors on cell surfaces, and under specific conditions such mechanical stimulations can activate cellular signaling pathways via receptor clustering, microtubule stimulation, and ion channel activation (Figure 7).[9b,20] Although multivalent biochemical ligands have the role to induce clusterization of the receptors in nature, magnetic nanoparticles can artificially induce the same

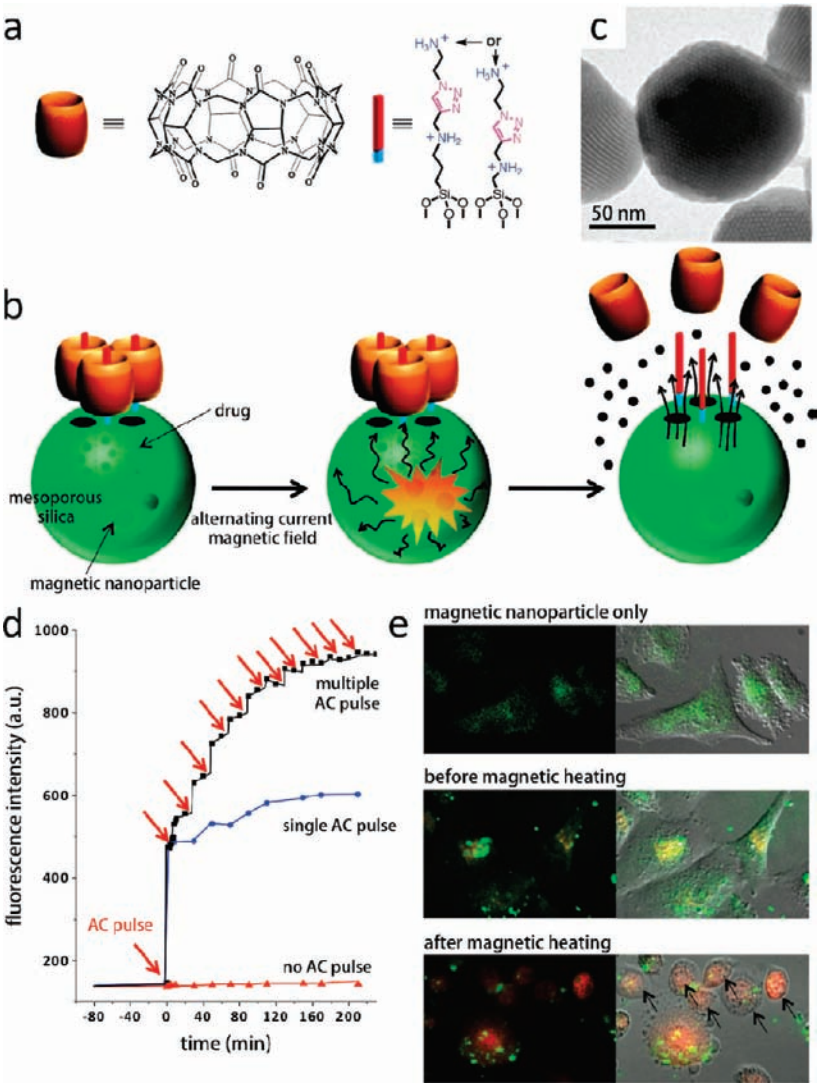

FIGURE 6. Magnetically triggered drug release system. (a) Chemical structure of thread and capping molecule (cucurbit[6]uril). (b) Schematics of nanoparticles, molecular machines, assembly, and remote-controlled drug release. The particles and machines are not drawn to scale. (c) TEM image of $(Zn_{0.4}Fe_{0.6})Fe_2O_4$ nanoparticles encapsulated mesoporous silica nanoparticles. (d) Drug release profile monitored during the AC field application with multiple AC field pulse (red arrows), single initial pulse, and no pulse. (e) Fluorescence image and differential interference contrast (DIC) image of MDA-MB-231 cancer cells treated by magnetic nanoparticles only and drug with the nanoparticles in silica carrier before and after the application of magnetic heating.

clusterization effects for cell signaling processes (Figure 8a).[21] Figure 8b shows the distribution of magnetic nanoparticles before and after the application of an external magnetic field. The magnetic nanoparticles are homogeneously distributed on the cell surface at first, but big clusters of magnetic nanoparticles are observed after the application of the magnetic field.

For effective magnetic manipulation, the design of the nanoparticles with a high magnetization value and superparamagnetism is critical. Some of the best suited nanoparticles are the 15 nm $(Zn_{0.4}Fe_{0.6})Fe_2O_4$ nanoparticles with a high magnetization value of 175 emu/g-magnetic atom, in which pico-Newton tensional forces can be applied by using a magnetic actuation setup with NdFeB magnets (Figure 8c). Then, we test magnetically induced angiogenesis which is one of the important processes related to new blood vessel formation in cancer biology. A TiMo214 monoclonal antibody (mAb) is conjugated to the 15 nm $(Zn_{0.4}Fe_{0.6})Fe_2O_4$ nanoparticle to target Tie2 receptors. Magnetically clustered Tie2 receptors on the cell surface initiate intracellular signal propagations, and key pathways such as phosphorylation of Tie2 (Figure 8d) and Akt (Figure 8e) are confirmed by Western blot and immunofluorescent techniques. In the Western blots (Figure 8d), a strong band for p-Tie2 is seen for the cells that are first treated with antibody conjugated Zn^{2+}-doped ferrite magnetic

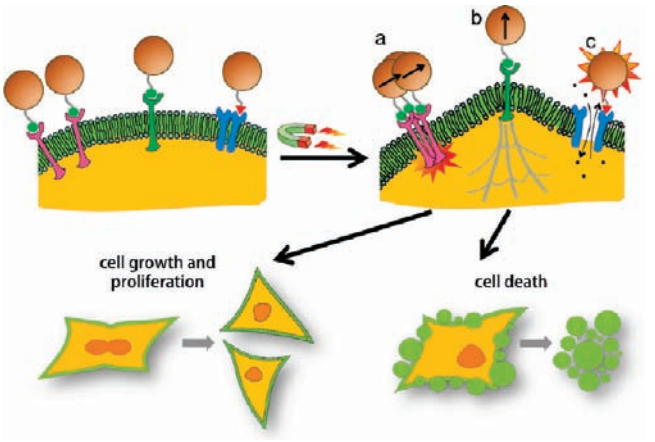

FIGURE 7. Magnetic activation of cell signaling. Magnetic nanoparticles conjugated with specific ligands can bind to receptors on cell surface. When an external magnetic field is applied, it can bring either (a) clusterizations, (b) pulling, or (c) heat generation of the nanoparticles that can cause a change in the cell fate such as growth and death.

nanoparticles (Ab-Zn-MNPs) and then the magnetic field is applied (Figure 8d). Phosphorylation of Akt (p-Akt) is confirmed by the observation of red fluorescence using anti-p-Akt immunoglobulin G and its secondary antibody, Alexa 594-labeled anti-rabbit IgG (Figure 8e). Such Tie2 receptor activations are further tested in human umbilical vein endothelial cells (HUVECs) and the expedited transformation of cellular morphology into a tubular shape is clearly observed under the influence of magnetic stimulation (Figure 8f). Such tubulogenesis is known to be the prestage of angiogenesis. Some of the advantages of the magnetically activated cellular transformation process over a conventional biochemical ligand system can be found in the new capabilities of the spatial, temporal, and remote control of cellular activities.

4.4. Magnetic Nanoparticles as a Delivery Carrier for Therapeutic Genes. Gene therapy is a new technique that uses genes to treat and prevent disease. siRNA is one of the

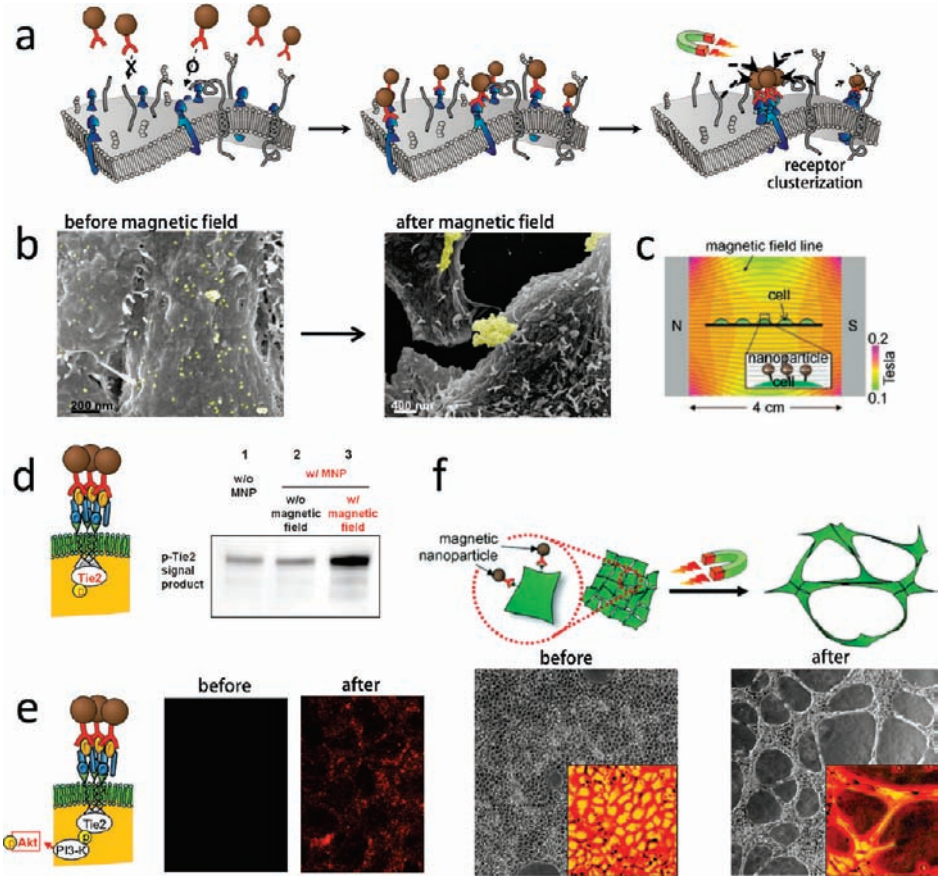

FIGURE 8. Activation of cellular signaling processes by magnetized nanoparticles. (a) Targeting and magnetic aggregation of cell surface receptors. (b) Scanning electron microscopy (SEM) image of before and after the magnetic field application. Nanoparticles are false-colored as yellow for clear visibility. (c) Magnet setup diagram for cell activations. (d) Phosphorylation of Tie2 (p-Tie2) and Western blot analysis. (e) Phosphorylation of Akt (p-Akt) and fluorescence confocal microscopy images of cell cytoplasm before and after application of a magnetic field. (f) Morphological change of HUVECs with Tie2 receptors before and after the application of magnetic field.

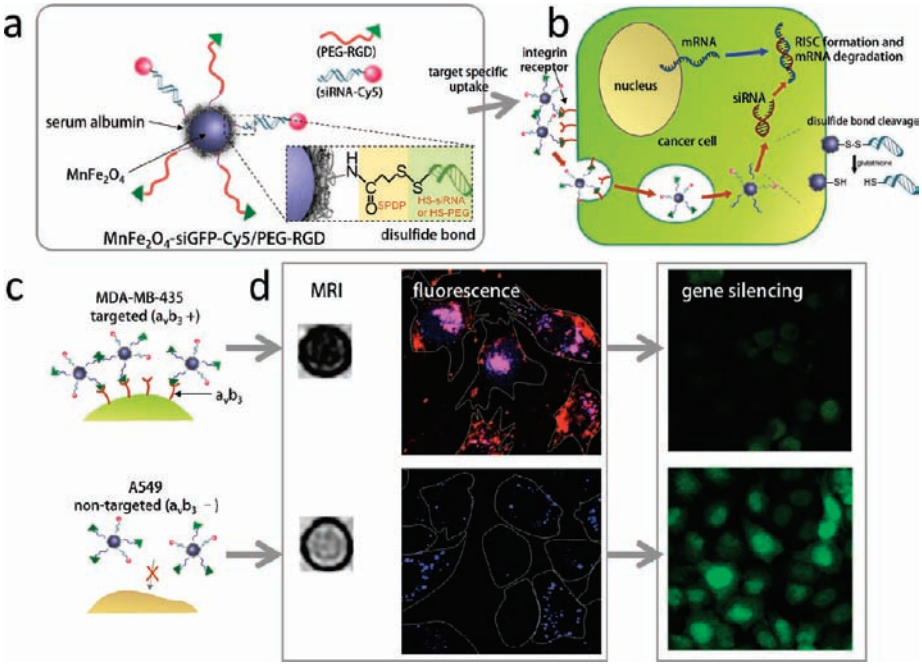

FIGURE 9. (a) Schematic drawing of all-in-one nanoparticles of $MnFe_2O_4$−siGFP−Cy5/PEG-RGD for theranostics. (b) Schematic illustration of intracellular processes of $MnFe_2O_4$−siGFP−Cy5/PEG−RGD nanoparticles, from target-specific uptake to mRNA degradation. (c) Schematic illustration of the target specific binding of the nanoparticles to $\alpha_v\beta_3$ integrin positive cells. (d) *T*2-weighted MR images of MDA-MB-435 and A549 cells treated with $MnFe_2O_4$−siGFP−Cy5/PEG−RGD. Confocal microscopy images showing the distribution of $MnFe_2O_4$−siGFP−Cy5/PEG−RGD nanoparticles in cells. Gene-silencing effect of the multimodal nanoparticle systems with ($MnFe_2O_4$−siGFP−Cy5/PEG−RGD) and without a targeting moiety ($MnFe_2O_4$−siGFP−Cy5/PEG) on $\alpha_v\beta_3$ integrin positive (MDA-MB-435) and $\alpha_v\beta_3$ integrin negative (A549) cell lines.

strong candidates for the next generation of gene therapy. siRNA binds mRNA to inhibit the translation processes of proteins in the cytoplasm.[22] Figure 9a shows a scheme for multifunctional magnetic nanoparticles for imaging and gene therapy. $MnFe_2O_4$ magnetic nanoparticles are conjugated with siRNA, fluorescence dye, surface stabilizing agent (polyethylene glycol, PEG), and targeting Arg-Gly-Asp (RGD) peptide.[23] RGD peptide targets $\alpha_v\beta_3$ integrin, which is overexpressed in certain endothelial and cancer cells. siRNA is bonded to nanoparticles via disulfide linkage which can be cleaved enzymatically for its facile release.[24] Multiple processes from target specific uptake of nanoparticles into the cells to siRNA release are shown in Figure 9b, in which nanoparticles recognize the cancer cells via targeting RGD peptide, and after endocytosed nanoparticles escape from the endosome, glutathione breaks the disulfide bond to release the siRNA for the inhibition of protein expression. The location of the therapeutic nanoparticles can be monitored via MRI and fluorescence techniques (Figure 9d). The selective targeting and theranostic of magnetic nanoparticles on $\alpha_v\beta_3$ receptor-expressing MDA-MB-435 human breast cancer cell lines are clearly shown with strong MRI signals and red fluorescence, and the gene silencing effect is apparent. In contrast, the control cell lines of receptor-free A549 do not show any such features. Since the endosome is stained as blue fluorescence, the red from the magnetic nanoparticles and blue fluorescence colocalize to emit yellow when the nanoparticles are inside the endosomes. However, after the nanoparticles escape the endosome, the two colors are seen separately. Red fluorescence in Figure 9d indicates that some nanoparticles successfully escape the endosome. Therapeutic efficacy is clearly observed from the suppression of GFP by the released siRNA for MDA-MB-435 cells, whereas bright green fluorescence is observed in the control cell line of A549 cells. This result demonstrates that magnetic nanoparticles can serve as platform materials for theranostics.

Contrary to gene suppression, gene expression in selective cell lines is also possible using magnetic nanoparticles. When adenovirus, which has target selectivity on cells expressing CAR receptor,[25] is coupled with magnetic nanoparticles, the success of gene delivery can be confirmed by MRI and fluorescence techniques.[26] Figure 10a shows the conjugation scheme of magnetic nanoparticles to adenovirus. The amino groups in the adenovirus and thiol group on the surface of the $MnFe_2O_4$ nanoparticles are connected using a cross-linker. As shown in Figure 10b, four or five magnetic nanoparticles are present per each adenovirus. Then, U251N cells with CAR expression and control CHO-1 cells are treated with the adenovirus−magnetic-nanoparticle

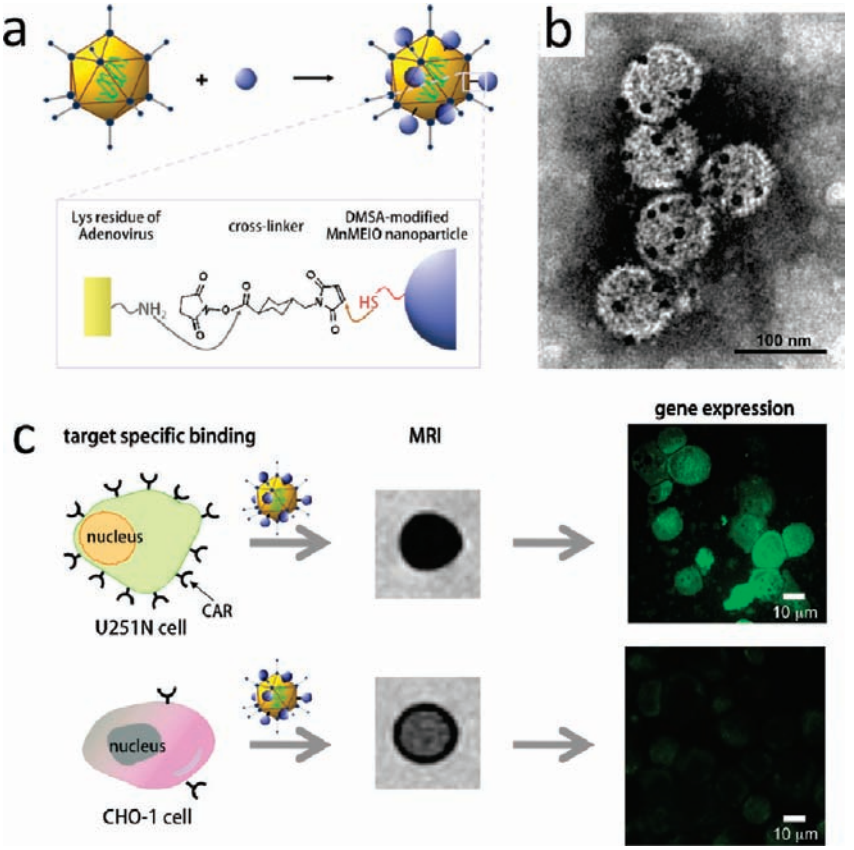

FIGURE 10. $MnFe_2O_4$-nanoparticle–adenovirus hybrids for MRI and efficient gene delivery. (a) Schematics showing the formation of $MnFe_2O_4$-nanoparticle–adenovirus hybrids. (b) TEM image of $MnFe_2O_4$-nanoparticle–adenovirus hybrids. (c) Target specific binding of the hybrid nanoparticles to CAR positive cells. *T*2-weighted MR images of U251N and CHO-1 cells treated with the hybrids. Fluorescence image of eGFP expression delivered by the hybrid nanoparticles.

conjugates (Figure 10c). For U251N cells, the *T*2 MRI signal is strong as a result of the binding of nanoparticles to the cells, while that of CHO-1 cells is weak. After endocytosis of adenovirus–magnetic-nanoparticle conjugates, the eGFP gene is successfully delivered to the nucleus to express GFP in the U251N cells where strong green fluorescence is observed.

5. Conclusions

Without a depth-penetration limit of the magnetic field in the human body, magnetic nanoparticles have been one of the ideal platform materials for targeted imaging of biological objects. Their additional capabilities are noninvasive and remote actuation for controlled drug release and cell signaling for therapeutics. These nanoparticles can also be used for targeted imaging of specific receptors and enzymes in disease processes and for the monitoring of the efficacy of the treatments. The current developmental stage of theranostic nanoparticles is still too early to predict their success, but rapid advances in new design concepts for next-generation nanoparticles have promising potential in that avenue.

BIOGRAPHICAL INFORMATION

Dongwon Yoo received his B.S., M.S., and Ph.D. degrees from Seoul National University in 1998, 2000, and 2004, respectively. He was a Postdoctoral Associate and a Research Staff Associate working with Professor Michael E. Jung at the University of California, Los Angeles (UCLA) and a recipient of the Molecular Biology Institute Postdoctoral Awards at UCLA (2010). He is currently a Research Professor at the National Center for Evolutionary Nanoparticles at Yonsei University.

Jae-Hyun Lee was born in Seoul, Korea and graduated from Yonsei University in 2003 with his B.S. He is a graduate student pursuing his Ph.D. in chemistry. His current research interests are the fabrication of hybrid magnetic nanoparticles for molecular imaging and therapeutics. He is a recipient of the Korea Research Foundation Fellowship (2004), Seoul Science Fellowship (2005), and Yonsei Graduate Student Research Award (2007).

Tae-Hyun Shin was born in Seoul, Korea. He earned his B.S. degree in chemistry from Yonsei University in 2010 and is a Ph.D. graduate student. His current research interest is the design and

construction of biocompatible inorganic nanocrystals for molecular and multimodal imaging.

Jinwoo Cheon is a Horace G. Underwood Professor at Yonsei University and the director of the National Creative Research Initiative Center for Evolutionary Nanoparticles. He graduated from Yonsei University with B.S. and received his Ph.D. from University of Illinois, Urbana−Champaign. After his postdoctoral training at U.C. Berkeley and at UCLA, he joined KAIST. In 2002, he moved to Yonsei University. He is a recipient of such awards as the Inchon Prize, Song-gok Award, and National Science Prize for Junior Faculty. Currently, he is a senior editor of *Accounts of Chemical Research* and an editorial board member of *Nano Letters* and *Journal of Materials Chemistry*.

FOOTNOTES

*To whom correspondence should be addressed. E-mail: jcheon@yonsei.ac.kr.

REFERENCES

1 (a) Ferrari, M. Cancer Nanotechnology: Opportunities and Challenges. *Nat. Rev. Cancer* **2005**, *5*, 161–171. (b) Peer, D.; Karp, J. M.; Hong, S.; Farokhzad, O. C.; Margalit, R.; Langer, R. Nanocarriers as an Emerging Platform for Cancer Therapy. *Nat. Nanotechnol.* **2007**, *2*, 751–760.

2 (a) Gradishar, W. J.; Tjulandin, S.; Davidson, N.; Shaw, H.; Desai, N.; Bhar, P.; Hawkins, M.; O'Shaughnessy, J. Phase III Trial of Nanoparticle Albumin-Bound Paclitaxel Compared With Polyethylated Castor Oil−Based Paclitaxel in Women With Breast Cancer. *J. Clin. Oncol.* **2005**, *23*, 7794–7803. (b) ClinicalTrials.gov, a service of the U.S. National Institute of Health. http://clinicaltrials.gov (accessed Feb 9, 2011).

3 (a) Alivisatos, A. P. Perspectives on the Physical Chemistry of Semiconductor Nanocrystals. *J. Phys. Chem.* **1996**, *100*, 13226–13239. (b) Link, S.; El-Sayed, M. A. Spectral Properties and Relaxation Dynamics of Surface Plasmon Electronic Oscillations in Gold and Silver Nanodots and Nanorods. *J. Phys. Chem. B.* **1999**, *103*, 8410–8426. (c) Jun, Y.-w.; Seo, J.-w.; Cheon, J. Nanoscaling Laws of Magnetic Nanoparticles and Their Applicabilities in Biomedical Sciences. *Acc. Chem. Res.* **2008**, *41*, 179–189.

4 (a) Pankhurst, Q. A.; Connolly, J.; Jones, S. K.; Dobson, J. Applications of Magnetic Nanoparticles in Biomedicine. *J. Phys. D: Appl. Phys.* **2003**, *36*, 167–181. (b) Lee, J.-H.; Huh, Y.-M.; Jun, Y.-w.; Seo, J.-w.; Jang, J.-t.; Song, H.-T.; Kim, S.; Cho, E.-J.; Yoon, H. G.; Suh, J.-S.; Cheon, J. Artificially Engineered Magnetic Nanoparticles for Ultra-Sensitive Molecular Imaging. *Nat. Med.* **2007**, *13*, 95–99.

5 (a) Cullity, B. D. *Introduction to Magnetic Materials*; Addison-Wesley Publishing: Reading, MA, 1972. (b) Spaldin, N. A. *Magnetic Materials: Fundamentals and Application*, 2nd ed.; Cambridge University Press: New York, 2010.

6 Fortin, J.-P.; Wilhelm, C.; Servais, J.; Ménager, C.; Bacri, J.-C.; Gazeau, F. Size-Sorted Anionic Iron Oxide Nanomagnets as Colloidal Mediators for Magnetic Hyperthermia. *J. Am. Chem. Soc.* **2007**, *129*, 2628–2635.

7 Rosensweig, R. E. Heating Magnetic Fluid with Alternating Magnetic Field. *J. Magn. Magn. Mater.* **2002**, *252*, 370–374.

8 Hergt, R.; Dutz, S. Magnetic Particle Hyperthermia—Biophysical Limitations of a Visionary Tumour Therapy. *J. Magn. Magn. Mater.* **2007**, *311*, 187–192.

9 (a) Sun, C.; Lee, J. S. H.; Zhang, M. Magnetic Nanoparticles in MR Imaging and Drug Delivery. *Adv. Drug. Deliv. Rev.* **2008**, *60*, 1252–1265. (b) Dobson, J. Remote Control of Cellular Behavior with Magnetic Nanoparticles. *Nat. Nanotechnol.* **2008**, *3*, 139–143.

10 Tong, S.; Hou, S.; Zheng, Z.; Zhou, J.; Bao, G. Coating Optimization of Superparamagnetic Iron Oxide Nanoparticles for High T_2 Relaxivity. *Nano Lett.* **2010**, *10*, 4607–4613.

11 Zborowski, M. Physics of Magnetic Cell Sorting. In *Scientific and Clinical Applications of Magnetic Carriers*, Häfeli, U., Schütt, W.,Teller, J., Zborowski, M.;Plenum Press: New York, 1997.

12 Smith, T. B.; Nayak, K. S. MRI Artifacts and Correction Strategies. *Imaging Med.* **2010**, *2*, 445–457.

13 Jang, J.-T.; Nah, H.; Lee, J.-H.; Moon, S. H.; Kim, M. G.; Cheon, J. Critical Enhancements of MRI Contrast and Hyperthermic Effects by Dopant-Controlled Magnetic Nanoparticles. *Angew. Chem., Int. Ed.* **2009**, *48*, 1234–1238.

14 Corot, C.; Robert, P.; Idèe, J.-M.; Port, M. Recent Advances in Iron Oxide Nanocrystal Technology for Medical Imaging. *Adv. Drug Delivery Rev.* **2006**, *58*, 1471–1504.

15 Choi, J.-s.; Lee, J.-H.; Shin, T.-H.; Song, H.-T.; Kim, E. Y.; Cheon, J. Self-Confirming "AND" Logic Nanoparticles for Fault-Free MRI. *J. Am. Chem. Soc.* **2010**, *132*, 11015–11017.

16 Medarova, Z.; Pham, W.; Farrar, C.; Petkova, V.; Moore, A. In vivo Imaging of siRNA Delivery and Silencing in Tumors. *Nat. Med.* **2007**, *13*, 372–377.

17 (a) Derfus, A. M.; Maltzahn, G. v.; Harris, T. J.; Duza, T.; Vecchio, K. S.; Ruoslahti, E.; Bhatia, S. N. Remotely Triggered Release from Magnetic Nanoparticles. *Adv. Mater.* **2007**, *19*, 3932–3936. (b) Hu, S.-H.; Chen, S.-Y.; Liu, D.-M.; Hsiao, C.-S. Core/Single-Crystal-Shell Nanospheres for Controlled Drug Release via a Magnetically Triggered Rupturing Mechanism. *Adv. Mater.* **2008**, *20*, 2690–2695.

18 Thomas, C. R.; Ferris, D. P.; Lee, J.-H.; Choi, E.; Cho, M. H.; Kim, E. S.; Stoddart, J. F.; Shin, J.-S.; Cheon, J.; Zink, J. I. Noninvasive Remote-Controlled Release of Drug Molecules in Vitro Using Magnetic Actuation of Mechanized Nanoparticles. *J. Am. Chem. Soc.* **2010**, *132*, 10623–10625.

19 (a) Zhu, C.; Bao, G.; Wang, N. Cell Mechanics: Mechanical Response, Cell Adhesion, and Molecular Deformation. *Annu. Rev. Biomed. Eng.* **2000**, *2*, 189–226. (b) Cartmell, S. H.; Keramane, A.; Kirkham, G. R.; Verschueren, S. B.; Magnay, J. L.; Haj, A. J. E.; Dobson, J. Use of Magnetic Particles to Apply Mechanical Forces for Bone Tissue Engineering Purposes. *J. Phys.: Conf. Ser.* **2005**, *17*, 77–80.

20 (a) Mannix, R. J.; Kumar, S.; Cassiola, F. V.; Montoya-Zavala, M.; Feistein, E.; Prentiss, M.; Ingber, D. E. Nanomagnetic Actuation of Receptor-Mediated Signal Transduction. *Nat. Nanotechnol.* **2008**, *3*, 36–40. (b) Lee, J.-H.; Kim, E. S.; Cho, M. H.; Son, M.; Yeon, S.-I.; Shin, J.-S.; Cheon, J. Artificial Control of Cell Signaling and Growth by Magnetic Nanoparticles. *Angew. Chem., Int. Ed.* **2010**, *49*, 5698–5702.

21 (a) Germain, R. N. T-Cell Signaling: The Importance of Receptor Clustering. *Curr. Biol.* **1997**, *7*, 640–644. (b) Cairo, C. W. Signaling by Committee: Receptor Clusters Determine Pathways of Cellular Activation. *ACS Chem. Biol.* **2007**, *2*, 652–655.

22 Brummelkamp, T. R.; Bernards, R. E.; Agami, R. Stable Suppression of Tumorigenicity by Virus-Mediated RNA Interference. *Cancer Cell* **2002**, *2*, 243–247.

23 Lee, J.-H.; Lee, K.; Moon, S. H.; Lee, Y.; Park, T. G.; Cheon, J. All-in-one Target-Cell-Specific Magnetic Nanoparticles for Simultaneous Molecular Imaging and siRNA Delivery. *Angew. Chem., Int. Ed.* **2009**, *121*, 4238–4243.

24 Derfus, A. M.; Chen, A. A.; Min, D.-H.; Ruoslahti, E.; Bhatia, S. N. Targeted Quantum Dot Conjugates for siRNA Delivery. *Bioconjugate Chem.* **2007**, *18*, 1391–1396.

25 (a) Hama, S.; Akita, H.; Ito, R.; Mizuguchi, H.; Hayakawa, T.; Harashima, H. Quantitative Comparison of Intracellular Trafficking and Nuclear Transcription between Adenoviral and Lipoplex Systems. *Mol. Ther.* **2006**, *13*, 786–794. (b) Bergelson, J. M.; Cunningham, J. A.; Droguett, G.; Kurt-Jones, E. A.; Krithivas, A.; Hong, J. S.; Horwitz, M. S.; Crowell, R. L.; Finberg, R. W. Isolation of a Common Receptor for Coxsackie B Viruses and Adenoviruses 2 and 5. *Science* **1997**, *275*, 1320–1323.

26 Huh, Y.-M.; Lee, E.-S.; Lee, J.-H.; Jun, Y.-w.; Kim, P.-H.; Yun, C.-O.; Kim, J.-H.; Suh, J.-S.; Cheon, J. Hybrid Nanoparticles for Magnetic Resonance Imaging of Target-Specific Viral Gene Delivery. *Adv. Mater.* **2007**, *19*, 3109–3112.